ISSN 1063-7761, Journal of Experimental and Theoretical Physics, 2023, Vol. 137, No. 4, pp. 494–505. © Pleiades Publishing, Ltd., 2023.
Russian Text © The Author(s), 2023, published in Zhurnal Eksperimental'noi i Teoreticheskoi Fiziki, 2023, Vol. 164, No. 4, pp. 571–583.

Structural Disorder, Specific Heat, and Magnetic Transitions in Cu_2FeBO_5

Yu. S. Gokhfeld[a,*], N. V. Kazak[a,], N. A. Bel'skaya[b], M. S. Molokeev[a,c], I. A. Gudim[a], O. A. Kondratiev[d], E. V. Eremin[a,c], Yu. V. Knyazev[a], D. A. Velikanov[a], and S. G. Ovchinnikov[a,c]**

[a] *Kirensky Institute of Physics, Federal Research Center Krasnoyarsk Science Center (KSC), Siberian Branch, Russian Academy of Sciences, Krasnoyarsk, 660036 Russia*

[b] *Ioffe Institute, St. Petersburg, 194021 Russia*

[c] *Siberian Federal University, Krasnoyarsk, 660041 Russia*

[d] *National Research Center Kurchatov Institute, Moscow, 123182 Russia*

**e-mail: yugo@krasn.ru*

***e-mail: nat@iph.krasn.ru*

Received March 30, 2023; revised June 3, 2023; accepted June 4, 2023

Abstract—Cu_2FeBO_5 ludwigite single crystals have been grown from a solution–melt by spontaneous crystallization. Using the X-ray diffraction method, the crystal structure has been resolved in detail. Cations in sites M2, M3, and M4 have turned out to be structurally disordered. It has been found that oxygen atoms are disordered in one of five nonequivalent sites (O4). As can be seen from Mössbauer spectroscopy data, Fe^{3+} ions occupy four nonequivalent sites with different distortions of coordination octahedra. In the temperature range 40 K ≤ T ≤ 300 K, the spectra represent a superposition of quadrupole doublets. Static susceptibility measurements have revealed two magnetic features at $T_1 = 35$ K and $T_2 = 20$ K and spin-glass effects. Specific heat measurements in the interval 4–300 K have not discovered magnetic-transition-related anomalies.

DOI: 10.1134/S1063776123100175

1. INTRODUCTION

Investigations of low-dimensional magnets are worthily considered as a mainstream in the theory of magnetism, to which L.A. Prozorova made an invaluable contribution [1–3]. In this article, we report research data on the oxyborates with a reduced-dimension magnetic subsystem. The anomalous behavior of the magnetization; spontaneous polarization; weak ferromagnetism; and structural, spin, and electronic transitions, along with other cooperative phenomena, heighten researchers' interest in these materials.

In oxyborates, the anion subsystem consists of "coupled" oxygen atoms, belonging to a boron–oxygen group, and "free" oxygen atoms. Strong O(2*p*)–B(2*p*) hybridization inside boron–oxygen complexes BO_3 or BO_4 provides structural ordering in the coupled anion subsystem. At the same time, free oxygen atoms make possible structural disordering and its related effects (structural and ferroelectric phase transitions, cation–anion conductivity, etc.).

Ludwigites with general formula of $Me_2^{2+}Me^{3+}(BO_3)O_2$ belong to the family of oxyborates in which the effects of anion and cation disordering considerably change the parameters of the magnetic and electronic subsystems. These materials crystallize in the orthorhombic system (space group symmetry *Pbam*). Metallic ions are coordinated by six oxygen atoms and occupy four nonequivalent crystal sites 2*a*, 2*b*, 4*g*, and 4*h* (which are usually designated as M1, M2, M3, and M4). In the overwhelming majority of heterometallic ludwigites, sites M2 and M4 are structurally disordered (Table 1). The maximal degree of structural disorder is observed in site M2 and may reach 100%.

In the ludwigites the cation distribution is the factor determining the ability of the system to reach long-range magnetic order. Investigations of Cu_2MnBO_5 using magnetic and neutron diffraction methods revealed the ferromagnetic ordering of spins below $T_N = 92$ K [6]. This compound is characterizied by the moderate cation disorder (Table 1). Spontaneous polarization ($P = 35$ μC/m^2 at 5 K) and incommensurable antiferromagnetic order below $T_N = 120$ K were discovered in cation-ordered Cu_2CrBO_5 [10]. In Cu_2GaBO_5, an intricate noncollinear antiferromagnetic order was observed at $T_N = 4.1$ K [11]. The low temperature of the magnetic transition was attributed to the influence of the disordered cation sublattice.

This article is devoted to studying mixed copper–iron ludwigite Cu_2FeBO_5. For the first time, its crystal

Table 1. Cationic disorder in the nonequivalent sites of the ludwigite lattice

	M1	M2	M3	M4
Cu_2GaBO_5 [4]	Cu(100%)	Cu(34%) + Ga(66%)	Cu(100%)	Cu(29%) + Ga(71%)
Cu_2AlBO_5 [5]	Cu(86%) + Al(14%)	Cu(34%) + Al(66%)	Cu(88%) + Al(12%)	Cu(33%) + Al(67%)
Cu_2MnBO_5 [6]	Cu(91%) + Mn(9%)	Cu(93%) + Mn(7%)	Cu(89%) + Mn(11%)	Cu(12%) + Mn(88%)
Cu_2FeBO_5 [4]	Cu(100%)	Cu(60%) + Fe(40%)	Cu(100%)	Cu(20%) + Fe(80%)
Ni_2AlBO_5 [7]	Ni(100%)	Ni(50%) + Al(50%)	Ni(100%)	Ni(25%) + Al(75%)
Co_2AlBO_5 [8]	Co(81%) + Al(19%)	Co(55%) + Al(45%)	Co(70%) + Al(30%)	Co(46%) + Al(54%)
Co_2GaBO_5 [9]	Co(100%)	Co(84%) + Ga(16%)	Co(100%)	Co(46%) + Ga(54%)

structure was resolved in [4]. The compound has monoclinic symmetry (space group $P2_1/c$). The symmetry reduction is due to the Jahn–Teller cooperative effect of Cu^{2+} ions. An anomalously high equivalent parameter of atomic displacement, $U_{eq}(O4) = 0.34(1)$ Å^2, was found, and a cationic disordering over M4 and M2 sites was established (Table 1). Later [12, 13], the magnetic properties were investigated. Measurements of the diamagnetic susceptibility and Mössbauer effect discovered three magnetic anomalies: at $T_N^{Fe} = 63$ K, the magnetic moments of iron ions freeze out; at $T_N^{Cu} = 35.7$ K, the antiferromagnetic order of spins in the copper subsystem sets in; and at $T = 20$ K, the magnetic moments of Fe^{3+} and Cu^{2+} ions are coupled in 3D network and a spin-glass state is onset. Based on the magnetic and Mössbauer effect measurements, it was found that Cu_2FeBO_5 undergoes an antifferomagnetic transition at $T_N = 32$ K [13]. From the Mössbauer spectrum quadrupole splittings, the following cation distributions were obtained: Cu : Fe = M1(0.40 : 0.10), M2(0.30 : 0.20), M3, M4(0.30 : 0.70) [12] and Cu : Fe = M1(0.26 : 0.24), M2(0.01 : 0.49), M3(0.75 : 0.25), M4(0.99 : 0.01) [13]. One can conclude that the metal ion distribution depends on the synthesis technique.

The present work is devoted to the study of the crystal structure and magnetic properties of a Cu_2FeBO_5 single crystals growing from the bismuth trimolybdate based flux. The elemental analysis of samples showed a high degree of cation stoichiometry. The measurements of single-crystal X-ray diffraction, Mössbauer effect, magnetization, and specific heat were carried out. It was found that iron ions, being in a high-spin trivalent state, occupy mainly M2 and M4 sites, thereby generating a considerable cation disorder. This disorder is associated with disordering in anionic site O4. The compound demostrates two magnetic transitions at $T_1 = 35$ K and $T_2 = 20$ K as well as a divergence of field-cooled (FC) and zero-field-cooled (ZFC) magnetization curves at $T < T_1$. The specific heat measurements did not reveal any anomalies associated with an emergence of the long-range magnetic order. This may indicate cation-disorder-induced exchange interaction frustrations.

2. EXPERIMENTAL AND ANALYTICAL METHODS

Cu_2FeBO_5 single crystals were grown from a solution–melt with the composition

$$68 \text{ wt } \% \ (Bi_2Mo_3O_{12} + Na_2B_4O_7 + CuO)$$

$$32 \text{ wt } \% \ (4CuO + Fe_2O_3 + B_2O_3).$$

Starting reagents (a total weight of 100 g) were sequentially melted in a 100-cm^3 platinum crucible at 1100°C. After homogenization for 3 h at 1000°C, the solution–melt was cooled to 925°C and then was slowly cooled at a rate of $dT/dt = 1$°C/day for two days. Subsequently, the liquid solution-melt was poured out. The single crystals grown on the crucible's walls were separated by etching in a 20% solution of nitric acid. The single crystals in form of the rectangular parallelepipeds had a typical size of $1.0 \times 1.0 \times 10.0$ mm^3.

The the sample's stoichiometry was determined by means of micro X-ray fluorescence analysis using a Bruker M4 Tornado fluorescence spectrometer. The operating parameters and conditions of the spectrometer were the following: Rh anode, accelerating voltage of 50 kV, current of 300 μA, and polycapillary focusing X-ray lens forming a light spot 25 μm in diameter. Both integral spectra with total sample surface mapping (with a step of 35 μm and an accumulation time of 80 ms per point) and subsequent averaging and spectra taken at a single point (with an accumulation time of 150 s) were recorded. To obtain quantitative data, spectra averaged over the sample surface and those recorded at a single point were analyzed with the Tornado M4 software package. With spectrometer precalibration taken into account, the determination inaccuracy of main component content is about 0.5% and the percentage of impurities less than 0.5% was determined qualitatively.

Diffraction intensities from a $0.1 \times 0.2 \times 0.3$-mm^3 Cu_2FeBO_5 single crystal were measured at $T = 296(2)$ K

Table 2. X -ray fluorescent analysis of the sample surface (map integrated spectrum)

Element	Atomic number	Series	Amount	wt %	Normalized wt %	Normalized at %
Mn	25	*K*-series	17888	0.023442	0.02385192	0.02648106
Ca	20	*K*-series	1270	0.006286	0.00639568	0.00973342
Cu	29	*K*-series	36584050	68.47264	69.6703074	66.8720291
Fe	26	*K*-series	25734015	29.77858	30.299445	33.0917564
Sum				98.28095	100	100

using a SMART APEX II single-crystal diffractometer (Bruker AXS, MoK_α radiation, analytical facility of the Krasnoyarsk center for collective use at the Common Access Facility Centres of SB RAS (Krasnoyarsk, Russia) with a CCD detector and a graphite monochromator. An orientation matrix and unit cell parameters were determined and refined for a set of 7361 reflections. The space group was found by statistically analyzing the intensities of all reflections. The absorption was taken into account using the SADABS program. The structure was resolved by direct methods from the SHELXS package and refined anisotropically using the SHELXL program [14]. Structural tests for missing symmetry elements and the presence of voids were conducted with the PLATON program [15]. Crystallographic data are deposited in the Cambridge Crystallographic Data Center (CSD no. 2252248).

The local distortions of coordination octahedra were analyzed in terms of the point charge model by calculating the principal component of the electric field gradient tensor [16]:

$$V_{zz} = 2e\sum_i \frac{3\cos^2\varphi_i - 1}{r_i^3}, \quad (1)$$

where φ_i is the angle between the major axis of the octahedron and the direction toward the ith oxygen atom and r_i are the corresponding cation–anion distances.

The valence states of iron ions were determined by the bond valence sum method [17]:

$$v_i = \sum_j \exp\frac{R_0 - r_{ij}}{b}, \quad (2)$$

where r_{ij} is the length of an i–j bond [Å]; parameter $R_0 = 1.759$ and 1.734 Å for Fe^{3+} and Fe^{2+} ions, respectively; and constant $b = 0.37$ Å.

Mössbauer spectra were recordered using a transmission-mode MS-1104Em spectrometer with a Co^{57} (Rh) radioactive source at 4, 40, and 300 K. Low-temperature measurements were made with a closed-cycle Gifford–McMahon cryostat. The isomer shifts of Mössbauer spectra were measured against a standard metallic α-Fe absorber. Hyperfine parameters were determined by the least-squares method under the assumption of Lorentzian line shape. Data were processed in two steps. First, possible nonequivalent sites of iron were revealed by calculating the probability-density distributions of the hyperfine field. According to results obtained at this step, a preliminary model spectrum was constructed. Then, model spectrum fits the experimental one by varying the entire set of hyperfine parameters with the least-squares method in a linear approximation.

The specific heat was measured on a single-crystal sample 10.66 mg in weight using a Quantum Design PPMS-9 (Common Access Facility Centres of SB RAS, Krasnoyarsk, Russia). The magnetization was measured using a SQUID magnetometer [18, 19] under FC and ZFC conditions in the temperature range 4–300 K at 200 Oe. Measurements were made on single-crystal powder samples with a total weight of 162 mg to minimize the influence of magnetic anisotropy.

3. RESULTS

Cu and Fe surface maps obtained by micro-X-ray fluorescence spectroscopy, as well as the map-integrated spectrum of the Cu_2FeBO_5, are shown in Fig. 1 and Table 2, respectively. The metal ions are distributed uniformly and the stoichiometry of the sample is high; namely, the ratio of metal ions is Cu : Fe = 2.02 ± 0.02.

The main crystallographic parameters, crystal structure refinement, as well as the atom's coordinates, site occupation factors, equivalent thermal parameters, and the main interatomic distances are listed in Tables 3–6. The lattice parameters a = 3.1271(3) Å, b = 12.0292(13) Å, c = 9.4813(10) Å, β = 97.045(2)°, and V = 353.35(6) Å^3, are in good agreement with those reported in [4].

Metal atoms are in an octahedral oxygen environment and occupy sites M1(2b), M2(2c), M3(4e), and M4(4e) (Fig. 2a). Oxygen atoms O2, O3, and O5 coordinate boron to form isolated planar triangular anions $(BO_3)^{3-}$. The remaining two atoms, O1 and O4, are "free" and coordinate metal ions. It was found that the O4 site splits into O4A and O4B sites spaced by 0.4604(56 Å) [4].

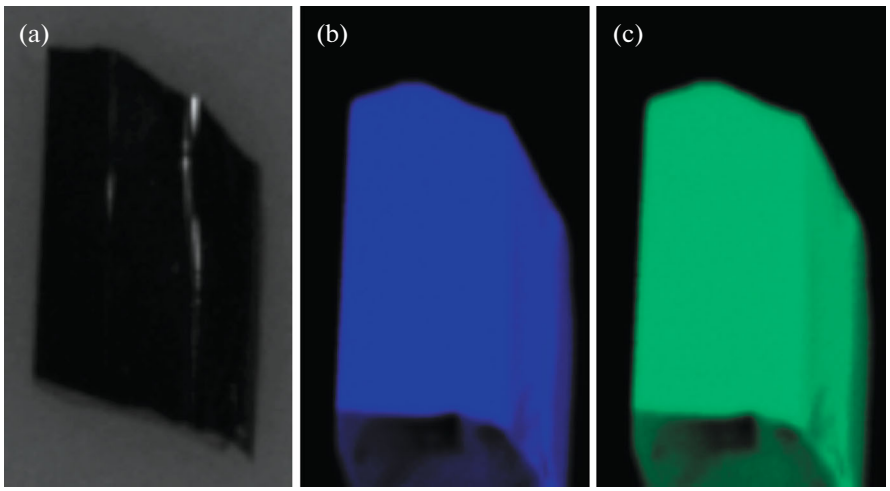

Fig. 1. (a) Image of the Cu_2FeBO_5 single crystal and (b) Cu and (c) Fe surface maps.

Copper and iron atoms at M2, M3, and M4 sites are structurally disordered with occupation factors of Cu : Fe = 0.496 : 0.504, 0.926 : 0.074, 0.328 : 0.672, respectively. Thus, the cation subsystem Cu_2FeBO_5 is divided into two sublattices: the first is structurally ordered Cu^{2+} ions at M1 and M3 sites (Fig. 2b), the second is the structurally disordered Cu^{2+}/Fe^{3+} ions at M2 and M4 sites (Fig. 2c). The edge-sharing octahedra $M2O_6$ and $M4O_6$ form triad M4–M2–M4 with the shortest interionic distance.

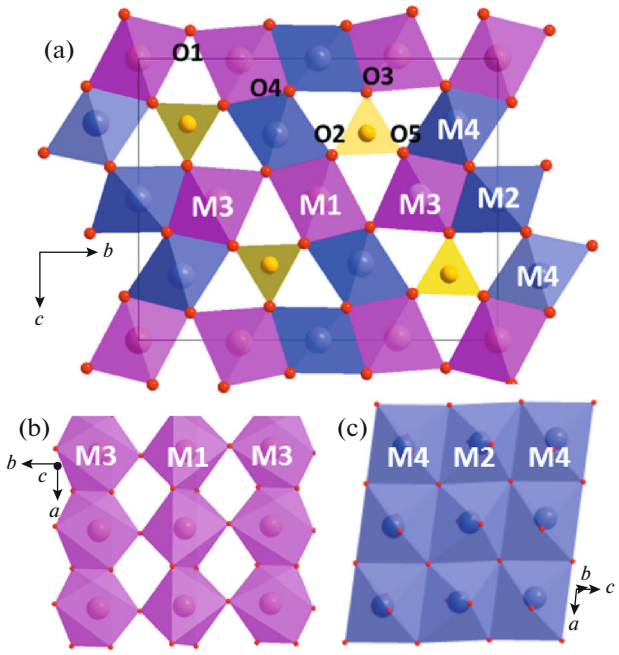

Fig. 2. (a) Projection of the Cu_2FeBO_5 crystal structure onto the *bc*-plane. Symmetrically nonequivalent sites occupied by metal ions are designated as M1–M4, and nonequivalent oxygen sites are designated as O1–O5. Yellow triangles are boron–oxygen groups. (b, c) Structurally ordered and structurally disordered magnetic subsystems formed by Cu^{2+} ions (sites M1 and M3) and Cu^{2+}/Fe^{3+} ions (sites M2 and M4), respectively.

The splitting of oxygen site O4 changes the local environment of transition ions and results in the distortion of the MeO_6 octahedra. The cationic disorder may be both dynamic and static. For statically disordered site O4, there are two sets of local environments for each of metal sites (M2A, M2B, M3A, M3B, M4A, and M4B), whereas for the dynamic disorder there appears many nonequivalent environments with different degrees of distortion of coordination octahedra.

Comparing the values of V_{zz}, one can see that the local distortions of coordination octahedra are characteristic of the statically disordered anion sublattice. Such disordering can be understood as a random distribution of the unit cells with oxygen atoms disordered over O4a or O4B sites. The considerable displacement of the O4B atom towards M4 site results in the shorteness of the corresponding M4–O4B = 2.0146(35) Å bond and simultaneous elongation of the M2–O4B = 2.5132(39) Å bond. For oxygen atoms occupying sites O4A, which are displaced toward atoms occupying sites M2, the effect was reverse: they elongate the bond M4–O4A = 2.6489(10) Å. The most regular oxygen environment arises at sites M2A and M4B (Table 7). They are also notable for the longest bond and, hence, for the highest charge states of Fe ions (2.84+ and 2.73+). The strongest distortions are observed at sites M1, M3A, and M3B occupied by Cu^{2+} ions. The symmetric environment of the Cu^{2+} ion with a degenerate ground state does not correlate with minimum energy. The degeneracy is removed by the Jahn–Teller effect. It is highly likely that the

Table 3. Crystal Data and Structure Refinement of Cu_2FeBO_5

Chemical formula	Cu_2FeBO_5
Molecular weight	273.735
Temperature, K	296(2)
Space group, Z	$P21/c$, 4
a, Å	3.1217(3)
b, Å	12.0292(13)
c, Å	9.4813(10)
β	97.042(2)°
V, Å^3	353.35(6)
ρ_{calc}, g/cm^3	5.146
μ, mm^{-1}	15.870
Measured reflections	7361
Independent reflections	1964
Reflections with $F > 2\sigma(F)$	1913
$2\theta_{max}$	$-5 \le h \le 5$; $-20 \le k \le 20$; $-16 \le l \le 16$
h, k, l – measurement limits	0.0460
R_{int}	0.0460
Processing F^2	$w = 1/[\sigma^2(F_0^2) + (0.0221P)^2 + 0.3824P]$, where $P = \max(F_0^2 + 2F_c^2)/3$
Number of processing parameters	93
$R1[F_0 > 2\sigma(F_0)]$	0.0286
$wR2$	0.0709
G_{oof}	1.243
$\Delta\rho_{max}$, e/Å^3	1.358
$\Delta\rho_{min}$, e/Å^3	−1.444
$(\Delta/\sigma)_{max}$	<0.001
Extinction coefficient (SHELXL 2014/7)	0.145(5)

Table 4. Atomic coordinates, parameters of isotropic displacement (U_{eq}), and SOFs of Cu_2FeBO_5

	x	y	z	U_{eq}	SOF
Cu1	0.5000	0.5000	0.5000	0.00664(8)	1
Cu2	0.0000	0.5000	0.0000	0.00643(10)	0.496(13)
Fe2	0.0000	0.5000	0.0000	0.00643(10)	0.504(13)
Cu3	0.45983(7)	0.28020(2)	0.00811(2)	0.00713(8)	0.926(8)
Fe3	0.45983(7)	0.28020(2)	0.00811(2)	0.00713(8)	0.074(8)
Cu4	0.06522(8)	0.61849(2)	0.72898(3)	0.00725(8)	0.328(9)
Fe4	0.06522(8)	0.61849(2)	0.72898(3)	0.00725(8)	0.672(9)
B	0.9623(6)	0.36378(15)	0.7330(2)	0.0070(3)	1
O1	0.5351(5)	0.64474(10)	0.59838(15)	0.0097(2)	1
O2	0.9620(4)	0.46083(10)	0.65647(13)	0.0081(2)	1
O3	0.0149(5)	0.36493(10)	0.87986(14)	0.0089(2)	1
O4A	0.5319(12)	0.4265(3)	0.1035(4)	0.0080(4)	0.503(5)
O4B	0.4201(12)	0.4154(3)	0.1277(4)	0.0080(4)	0.497(5)
O5	0.9084(5)	0.23690(11)	0.16530(14)	0.0094(2)	1

Table 5. Parameters of anisotropic displacement of Cu_2FeBO_5

	U^{11}	U^{22}	U^{33}	U^{23}	U^{13}	U^{12}
Cu1	0.00849(13)	0.00456(13)	0.00626(13)	−0.00101(7)	−0.00154(9)	0.00044(8)
Cu2	0.00819(15)	0.00445(14)	0.00623(15)	−0.00041(8)	−0.00076(10)	0.00096(8)
Fe2	0.00819(15)	0.00445(14)	0.00623(15)	−0.00041(8)	−0.00076(10)	0.00096(8)
Cu3	0.00986(11)	0.00403(11)	0.00664(11)	−0.00085(5)	−0.00239(7)	0.00098(6)
Fe3	0.00986(11)	0.00403(11)	0.00664(11)	−0.00085(5)	−0.00239(7)	0.00098(6)
Cu4	0.00954(12)	0.00457(11)	0.00692(11)	−0.00110(6)	−0.00189(7)	0.00030(6)
Fe4	0.00954(12)	0.00457(11)	0.00692(11)	−0.00110(6)	−0.00189(7)	0.00030(6)
B	0.0079(6)	0.0056(6)	0.0070(6)	0.0007(5)	−0.0010(5)	−0.0003(5)
O1	0.0129(5)	0.0044(5)	0.0105(5)	−0.0002(4)	−0.0042(4)	0.0000(4)
O2	0.0113(5)	0.0041(4)	0.0079(5)	0.0005(3)	−0.0024(4)	−0.0008(3)
O3	0.0131(5)	0.0063(5)	0.0065(5)	−0.0001(3)	−0.0021(4)	0.0014(4)
O4A	0.0102(13)	0.0053(8)	0.0075(11)	−0.0001(7)	−0.0024(7)	0.0007(8)
O4B	0.0102(13)	0.0053(8)	0.0075(11)	−0.0001(7)	−0.0024(7)	0.0007(8)
O5	0.0147(5)	0.0052(4)	0.0073(5)	0.0002(4)	−0.0031(4)	0.0019(4)

anomalous bond elongation and high values of V_{zz} at sites M2B and M4A are associated with Cu^{2+} ions at these sites. From the above analysis it follows that the unit cell may contain triads of two types: Fe(4A)–Fe(2A)–Cu(4A) and Fe(4B)–Cu(2B)–Fe(4B) (Fig. 3). A random distribution of such triads in the lattice generates the effect of cationic disorder with site occupancy factors (SOFs) Cu2 : Fe2 = 0.5 : 0.5 and Cu4 : Fe4 = 0.25 : 0.75. These values are close to experimentally found populations (0.496 : 0.504 and 0.328 : 0.672, respectively).

Table 6. Main interatomic distances in Cu_2FeBO_5

Bond	Bond length
Cu1–O1	2 × 1.9719(13)
Cu1–O2	4 × 1.9945(12)
Cu2|Fe2–O3	2 × 1.9881(13)
Cu2|Fe2–O4A/O4B	2.0253(36)/1.9575(36)
Cu2|Fe2–O4A/O4B	2 × 2.0571(39)/2.5132(39)
Cu3|Fe3–O1	1.9180(13)
Cu3|Fe3–O3	2.0081(14)
Cu3|Fe3–O3	2.4570(15)
Cu3|Fe3–O4A/O4B	1.9788(36)/1.9951(37)
Cu3|Fe3–O5	1.9853(14)
Cu3|Fe3–O5	2.4668(16)
Fe4|Cu4–O1	1.9670(14)
Fe4|Cu4–O1	2.0567(16)
Fe4|Cu4–O2	2.0295(12)
Fe4|Cu4–O5	2.0043(14)
Fe4|Cu4–O4A/O4B	1.9767(36)/2.0146(35)
Fe4|Cu4–O4A/O4B	2.6489(40)/2.1939(40)
B–O2	1.3745(22)
B–O3	1.3820(23)
B–O5	1.3713(22)

The Mössbauer spectrum of the Cu_2FeBO_5 sample (Fig. 4a) taken at room temperature can be satisfactorily approximated by a sum of four quadrupole doublets (Table 8). The hyperfine parameters are in good agreement with those reported earlier [12, 13]. The isomer shift values, $IS = 0.356–0.454$ mm/s, are typical for high-spin Fe^{3+} ions in the octahedral oxygen coordination. Unlike the X-ray diffraction, that is an integral method, the Mossbauer spectroscopy is a high selectivity method and more sensitive to the iron atom local environment. A row a discrete values of the quadrupole splittings points out the different iron sites relative to the local environment. The quadrupole splitting of $QS1 = 2.04$ mm/s is an indication that iron ions occupy highly distorted octahedra. A small area of this component ($A1 = 5\%$) implies an atypical (random) distribution of Fe^{3+} ions in this site. Such a component was observed earlier in the spectra of Ni_2FeBO_5 ($QS = 1.93$ mm/s, $A = 6\%$ [20] and $Co_{3-x}Fe_xBO_5$ with $0.0 < x \leq 1.0$ ($QS = 1.96–1.92$ mm/s, $A = 20–10\%$ [21]). Spectral component D4, which is characterized by a small quadrupole splitting ($QS4 = 0.62$ mm/s), may be assigned to iron ions in the most regular ligand environment. The most probable distribution of Fe^{3+} ions is a distribution over moderately distorted octahedral sites with a quadrupole splitting in the interval 0.8–1.2 mm/s. Assuming that in magnetic insulators the valence contribution to the electric field gradient is small and the ligand contribution is the main one, the quadrupole splitting on the iron nuclei is proportional to the main component

Table 7. Mean bond length, main component of the electric field gradient tensor, and valence states of iron ions in nonequivalent sites of the Cu_2FeBO_5 lattice

	M1	M2A	M3A	M4A	M2B	M3B	M4B
⟨Me–O⟩, Å	2.1287	2.0235	2.1357	2.1139	2.1529	2.1384	2.0443
V_{zz}, e/Å^3	−0.440	−0.030	−0.499	−0.271	−0.535	−0.519	−0.087
Valence state Fe		2.84		2.57	2.42		2.73

of the electric field gradient induced by the oxygen atoms. One can assign spectral components to crystallographic sites using the values of V_{zz} calculated for different local atomic configurations (Table 8). The total area of doublets D2 (36%) and D3 (43%) is close to the site occupation factor of the nonequivalent M4 site determined from X-ray diffraction data (≈67%), and corresponds to the theoretical occupation assuming the static disorder (75%).

In [12] a considerable broadening of Mössbauer spectral lines at $T < 60$ K was reported. This finding was attributed to the relaxation effect and freezing-out of iron magnetic moments. Figure 4b shows the Cu_2FeBO_5 spectrum taken at 40 K. Unlike data obtained in [12], the spectral profile is described, by a sum of four components with occupations factors D1 : D2 : D3 : D4 = 6 : 38 : 42 : 14 assuming the paramagnetic state of Fe^{3+} ions at this temperature.

At $T = 4$ K, Zeeman splitting of lines is observed (Fig. 4c). The spectrum is approximated by a sum of three sextets. The spectral components in the magntically ordered phase and paramagnetic state were relared using the spectral areas.

The sextets S2, S3, and S4 were assigned the occupation factors 0.33, 0.53, and 0.14, respectively. The *IS* values grow, becoming typical of Fe^{3+} ions. Hyperfine fields at iron nuclei were $H_{hf} = 479$ (*S*1), 459 (*S*2), and 421 (*S*3) kOe. The mean hyperfine field $\langle H_{hf} \rangle$ = 460 kOe, is close to 469 kOe given in [12] but is much lower than those found for Co_2FeBO_5 (508 kOe) [21] and Fe_3BO_5 (500 kOe) [22]. This implies incomplete magnetic ordering in the Fe sublattice possibly due to the cation-disorder-induced frustrations of exchange interactions.

The temperature dependences of the Cu_2FeBO_5 magnetization taken at 200 Oe are presented in Fig. 5. A peak of magnetization is observed at the temperature $T_1 = 35$ K, below which the FC and ZFC curves diverge. At $T < T_1$, the FC magnetization tends to a constant value and the ZFC curve changes the slope at $T = 20$ K (the lower inset to Fig. 5). Two features similar to those observed in our experiments were reported earlier in work [12] where the dynamic magnetic susceptibility of Cu_2FeBO_5 was measured (T_N^{Cu} = 35.7 K and $T = 20$ K). The high-temperature feature at $T_N^{Fe} = 63$ K, assigned to the freezing-out of the Fe subsystem magnetic moments [12], does not observed in our magnetic measurements.

At high temperatures, the magnetic susceptibility obeys the Curie–Weiss law

$$\chi(T) = \chi_0 + \frac{C}{T - \Theta}, \qquad (3)$$

where χ_0 is a temperature-independent contribution, C is the Curie constant, Θ is the paramagnetic Curie temperature. Temperature-independent contribution $\chi_0 = \chi_{dia} + \chi_{VV}$ represents a sum of diamagnetic contribution, which, in turn, is a sum of negative Pascal constants ($\chi_{dia} = -35 \times 10^{-6}$, -12×10^{-6}, and -10×10^{-6}

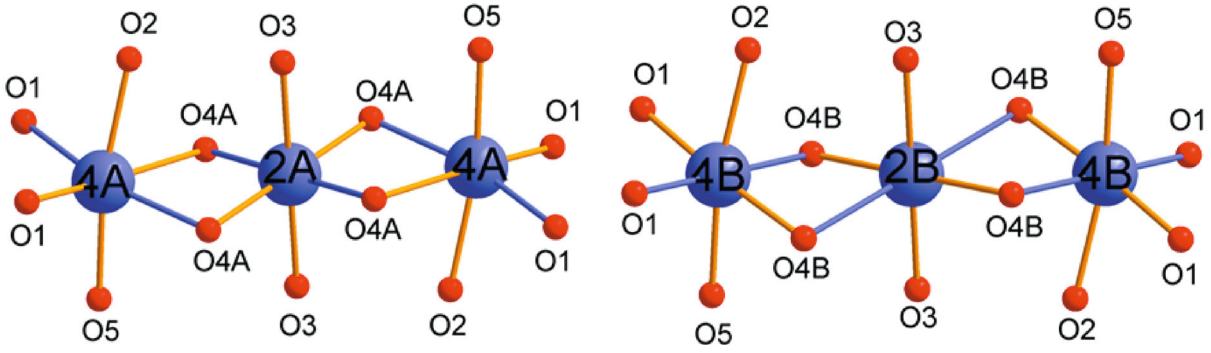

Fig. 3. Coordination environment of metal ions in the statically disordered subsystem of Cu_2FeBO_5: the unit cell is ordered in oxygen sites O4A and O4B. The axial elongation of octahedra is colored.

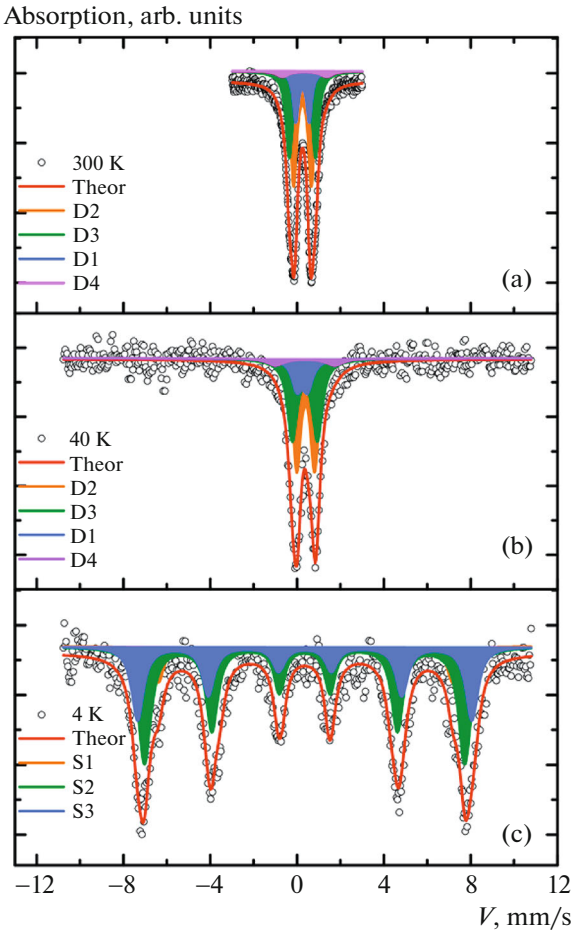

Fig. 4. Mössbauer spectra of Cu_2FeBO_5 taken at (a) 300, (b) 40, and (c) 4 K.

cm^3/mol for $(BO_3)^{3-}$, Cu^{2+}, and Fe^{3+}, respectively), and the positive Van Vleck contribution determined for a Cu^{2+} ion in the cubic crystal field as $\chi_{VV} \approx 50 \times 10^{-6}$ cm^3/mol [24]. The fitting of the experimental data in the temperature range $T > 180$ K accounting the contribution $\chi_0 = 0.3 \times 10^{-4}$ cm^3/mol yields a lager-in-modulus negative Curie temperature, $\Theta = -429$ K. This value is much higher (in modulus) than those reported in other publications (−178 K [12] and −384 K [13]). At $T < 160$ K, i.e., at a temperature much higher than the magnetic transition temperature, the magnetic susceptibility deviates from the Curie–Weiss law, assuming the development of the short-range magnetic correlations (the upper inset to Fig. 5). At $T < T_1$, the antiferromagnetic exchange correlations predominate. The effective magnetic moment turns out to be $\mu_{eff} = 6.16$ μ_B/f.u. This value agrees well with the theoretical one,

$$\mu_{eff} = \sqrt{2\mu_{Cu}^2 + \mu_{Fe}^2} = 6.4\ \mu_B/\text{f.u.}, \qquad (4)$$

assuming that Cu^{2+} and Fe^{3+} ions are in high-spin states ($S = 1/2$ and 5/2, respectively) and the g-factor $g = 2$.

Figure 6 presents the zero-field temperature dependence of the specific heat for the Cu_2FeBO_5 single crystal. Importantly, the magnetic transitions at T_1 and T_2 found from static magnetization measurements do not manifest themselves as anomalies in the temperature dependence of the specific heat, which is a monotonically varying function throughout the measuring interval.

The room-temperature specific heat equals 166.4 J/(mol K), which is much lower than the Dulong–Petit thermodynamic limit: $3Rz = 224.5$ J/(mol K), where R is the gas constant and z is the number of atoms per formula unit. The magnetic contribution to the specific heat was obtained by subtracting lattice contribution C_{latt}, which was approximated by the Debye–Einstein function. The Debye temperature was found to be $\Theta_D = 398 \pm 20$ K. The magnetic contribution to the entropy saturates at $T \approx 100$ K, $S_{mag} \approx 7$ J/(mol K) (an inset to Fig. 6). This value is much lower than the theoretical one:

$$S_{mag} = 2R\ln(2S_{Cu} + 1) + R\ln(2S_{Fe} + 1) = 24.4\ \text{J/(mol K)}. \qquad (5)$$

The absence of anomalies associated with the long-range magnetic order and the low value of S_{mag} may indicate exchange interaction frustrations and the formation of the short-range order at higher temperatures.

4. DISCUSSION

Recent neutron diffraction experiments with Cu_2GaBO_5 have shown that at $T_N = 4.1$ K a commensurable antiferromagnetic order with magnetic propagation vector $\mathbf{q}_m = (0.45, 0, -0.7)$ arises [11]. The magnetic subsystem consists of two sublattices, one being formed by structurally ordered Cu^{2+} ions in M1 and M3 sites and the other by structurally disordered Cu^{2+} and Ga^{3+} ions in M2 and M4 sites. The magnetically diluted sublattice either does not participate in antiferromagnetic ordering, remaining in the paramagnetic state below T_N, or inherits the antiferromagnetic correlations of the ordered sublattice due to the low number of exchange bonds due to cationic disorder. In absence of an external field, such disordered sublattice does not make a considerable contribution to the magnetic energy of the system, allowing the formation of the long-rage order in the structurally and magnetically ordered sublattice of Cu^{2+} spins. This is corroborated by the presence of a λ-anomaly in the temperature dependence of the specific heat. In an external field, the spin polarization of the disordered sublattice leads to the suppression of the long-range order in the ordered sublattice.

Table 8. The hyperfine structure parameters of Cu_2FeBO_5: *IS*, measured chemical shift relative to α-Fe (±0.05 mm/s); H_{hf}, hyperfine field (±3 kOe); *QS*, quadrupole splitting (±0.01 mm/s); *W*, full width at half maximum (±0.001 mm/s); *A*, area under the spectral component (±3%)

T, K	Coordinates	*IS*, mm/s	H_{hf}, kOe	*QS*, mm/s	*W*, mm/s	*A*, %	Site
300	D1	0.454		2.04	0.63	5	3
	D2	0.356		1.20	0.37	36	4A
	D3	0.359		0.81	0.34	43	4B
	D4	0.358		0.62	0.29	16	2A
40	D1	0.475		2.74	0.92	6	
	D2	0.461		1.15	0.54	38	
	D3	0.501		0.82	0.43	42	
	D4	0.348		0.50	0.56	14	
4	S2	0.467	479	–0.02	0.66	33	
	S3	0.457	459	0	0.57	53	
	S4	0.490	421	0.00	0.42	14	

The high-in-modulus and negative value of Θ = –429 K, indicates a high magnitude of antiferromagnetic interactions. On the other hand, the absence of the specific heat anomalies may indicate that long-range magnetic order does not form. Such behavior means that exchange interactions are suppressed, possibly, due to the strong frustrations of the exchange interactions. Comparing the values of Θ for Cu_2FeBO_5 and Cu_2GaBO_5 (–60 K) [5, 11], one can see that the substitution of nonmagnetic Ga^{3+} ions for magnetoactive Fe^{3+} ions enhances antiferromagnetic correlations. The ratio between Curie temperature Θ and magnetic transition temperature T_{cr} ($\Theta/T_{cr} \approx 12$ and 15 for Ga- and Fe-substituted samples, respectively) suggests that magnetic frustrations in both materials are generated by the structurally and magnetically disordered sublattice M4–M2–M4. A rise in the mean magnetization of such a sublattice owing to magnetic substitution is expected to increase the contribution of this subsystem to the total magnetic

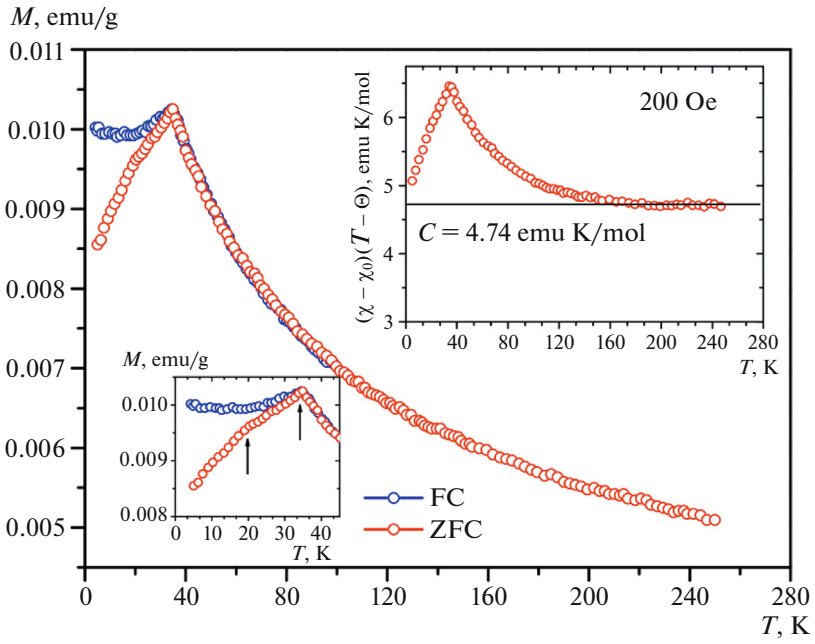

Fig. 5. Temperature dependences of the Cu_2FeBO_5 magnetization taken under FC and ZFC conditions in a field of 200 Oe. The lower inset shows the magnetic transition range on an enlarged scale (magnetic anomalies are marked by arrows). The upper inset plots the function $(\chi - \chi_0)(T - \Theta)$ vs. *T*. The continuous line is the plot of the Curie constant.

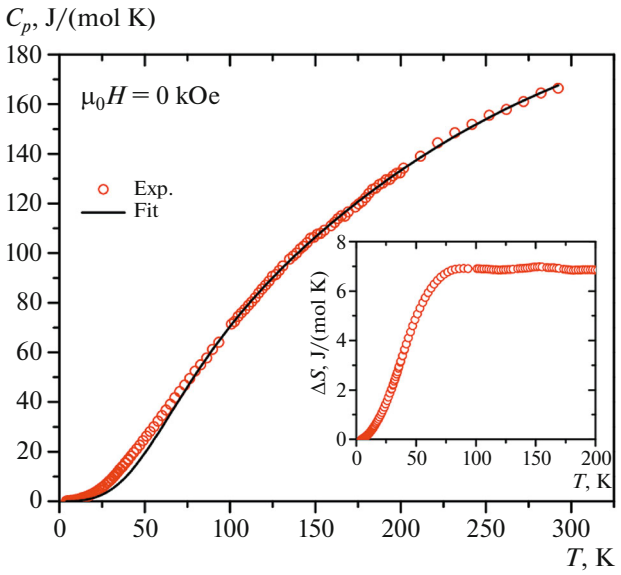

Fig. 6. Temperature dependence of the specific heat of single-crystalline Cu_2FeBO_5. The continuous line approximates the lattice contribution to the specific heat. The inset shows the temperature dependence of the entropy.

energy. Its influence on the ordered subsystem increases so that the long-range order is suppressed. The strong dependences of the magnetization on cooling conditions (FC or ZFC) in low fields and the absence of specific heat anomalies count in favor of the fact that a state similar to spin glass forms in Cu_2FeO_5 at $T_1 = 35$ K. The rise of magnetic transition temperature T_1 compared with T_N in Cu_2GaBO_5 [5, 11, 13] is reflective of the emerging role of the structurally disordered subsystem. In Cu_2FeBO_5 the frustrations leads to the release of a significant part of the magnetic entropy at high temperatures, which is manifested in measurements of heat capacity and magnetic susceptibility.

Thus, the ludwigites represent an example of the experimental implementation of systems with a strong interrelation of the structural and magnetic orders. Because of this, controlling the structural order, one gets a chance to control magnetic and electron properties. Disordering in the cationic subsystem may result from disordering in the anionic one. In the ludwigite structure, three of five symmetrically nonequivalent oxygen sites belong to the BO_3 triangle and therefore to the rigid framework of the anion subsystem. The displacement of these atoms is expected to distort BO_3 triangles, namely, cause their rotation about or deviation from the *bc* plane, that is, radically change the crystal structure. At the same time, the atoms O1 and O4 are "free," from which only atom O4 has the highest mobility (anomalously large parameter U_{eq}).

The atomic instability of site O4 is associated with its nonequivalent cationic environment in respect of other oxygen sites. Table 9 lists oxygen–cation interionic distances and mean distances ⟨O–Cation⟩ for each site. The nearest-neighbor environment of atoms O2, O3, and O5 contains, together with the boron atom, three metal ions. These sites are characterized by the smallest ⟨O–Cation⟩ distances: 1.955, 1.959, and 1.957 Å, respectively. Oxygen atom O1 has four bonds with metal atoms. The bond lengths are close to each other with a mean ⟨O–Cation⟩ bond length of 1.978 Å. Split oxygen site O4A/O4B is coordinated by the greatest number of metal atoms (five atoms). With such a coordination, an O^{2-} anion produces five bonds with a mean strength of 0.4 of a valence unit. This value is smaller than for oxygen atoms O1, O2, O3, and O5 (a mean strength of 0.5 of a valence unit). Therefore, for the oxygen atom in site O4, the ⟨O4–Cation⟩ bond length lies in the interval 2.135–2.137 Å. This value is much greater than that for other oxygen atoms. It is likely that weakening of interactions due to the considerable bond elongation causes the atomic instability of this site. Since oxygen atom O4 can displace toward a metal atom, the symmetry of the crystal field near the Cu^{2+} cation reduces and, conversely, the local symmetry of the octahedron around Fe^{3+} ions (*S* ions) increases. The alternation of charges along the "ordered" chain of ions M4–M2–M4 is expected to decrease the total energy of the system due to the gain in stabilization energy, which minimizes due to ordering of distortions.

The atomic instability of site O4 may explain disorder in the cationic subsystem. The more oxygen atoms coordinating the metal, which is structurally disordered, the greater the structural disorder at the given metallic site. In the nearest-neighbor environment of the metal ion in site M2, four of six oxygen atoms are disordered in relation to site O4 ($\delta = 2/3$). For metal ions in sites M4 and M3, this ratio is 1/3 and 1/6, respectively. From this a condition for cation disorder follows according to which the degree of disorder decreases in the sequence M2 > M4 ≫ M3 in good agreement with the experimental SOF found from X-ray diffraction and Mössbauer spectroscopy data obtained for heterometallic compounds from the ludwigite family (Table 1).

The results of this study demonstrate that the magnetic state of the ludwigites in general and Cu_2FeBO_5 in particular strongly depends on the cationic distribution, which, in turn, is extremely sensitive to synthesis conditions (synthesis method, solution–melt system, crystallization temperature, cooling rate, etc.). The increase in the local symmetry of octahedra induced by anion ordering may equalize potentials between occupied metal sites and redistribute cation states. In view of the aforesaid, it was of interest to investigate the crystal structure and electronic properties of ludwigites at high temperatures.

An alternative way to control cations and, hence, magnetic order, is using the transition metal ions with

Table 9. Bond lengths in the cationic environment of oxygen atoms in Cu_2FeBO_5. The mean bond-lengths are in bold

Bond	Length, Å	Bond	Length, Å	Bond	Length, Å
O1–Cu1	1.9719(13)	O2–Cu1	1.9945(12)	O3–Cu2|Fe2	1.9881(13)
O1–Cu3	1.9180(13)	O2–Cu1	2.4197(13)	O3–Cu3	2.0081(14)
O1–Fe4|Cu4	1.9670(14)	O2–Fe4|Cu4	2.0295(12)	O3–Cu3	2.4570(15)
O1–Fe4|Cu4	2.0567(16)	O2–B	1.3745(22)	O3–B	1.3820(23)
⟨O1–Cation⟩	**1.9784**	**⟨O2–Cation⟩**	**1.9546**	**⟨O3–Cation⟩**	**1.9588**
O4A–Cu2|Fe2	2.0253(36)	O4B–Cu2|Fe2	1.9575(36)	O5–Cu3	1.9853(14)
O4A–Cu2|Fe2	2.0571(39)	O4B–Cu2|Fe2	2.5132(39)	O5–Cu3	2.4668(16)
O4A–Cu3	1.9788(36)	O4B–Cu3	1.9951(37)	O5–Fe4|Cu4	2.0043(14)
O4A–Fe4|Cu4	1.9767(36)	O4B–Fe4|Cu4	2.0146(35)	O5–B	1.3713(22)
O4A–Fe4|Cu4	2.6489(40)	O4B–Fe4|Cu4	2.1939(40)		
⟨O4A–Cation⟩	**2.1374**	**⟨O4B–Cation⟩**	**2.1349**	**⟨O5–Cation⟩**	**1.9569**

incompletely filled 4*d*- and 5*d*-shells (Nb^{5+}, Ta^{5+}, W^{6+})—so-called ferroelectric ions. Strong covalent bonding between this ion and environmental oxygen ions may provide the atomic stability of oxygen sites and, correspondingly, the structural order in the anion subsystem. A successful implementation of such approach is recently synthesized warwickite $Co_{1.33}Nb_{0.67}BO_4$, in which the long-range ferromagnetic order can be reached by passing through two phase transitions [25].

5. CONCLUSIONS

Cu_2FeBO_5 ludwigite single crystals were grown by spontaneous crystallization from a solution–melt. The crystal structure was resolved by the X-ray diffraction method. The structural disordering of Cu and Fe atoms, which arises mainly in the M4–M2–M4 triad, was discovered. It results from the structural disordering of oxygen atoms in site O4. The displacement of oxygen atoms in site O4 reduces the crystal field symmetry at the site occupied by a Cu^{2+} ion and increases the symmetry at the site occupied by a Fe^{3+} ion. As a result, the unit cell contains triads of two types, Fe(4A)–Fe(2A)–Cu(4A) and Fe(4B)–Cu(2B)–Fe(4B), in which oxygen atoms are statically ordered. Mössbauer measurements showed that Fe^{3+} ions, being in the octahedral environment, are in the high-spin state and occupy four nonequivalent (in local environment) sites. The paramagnetic state of iron ions persists up to 40 K. The spectrum taken at 4 K is approximated by a sum of three sextets with mean hyperfine field at iron nuclei $\langle H_{hf}\rangle = 460$ kOe. Static magnetization measurements revealed the divergence of FC and ZFC curves in low fields and two magnetic features at 35 and 20 K. The absence of magnetic-transition-induced anomalies of the specific heat and a small value of the magnetic entropy, $S \approx 7$ J/(mol K), suggest the dominance of the short-range magnetic order and the presence of frustrations due to cationic disordering in the subsystem. Ways to achieve the cationic order and long-range magnetic order are under discussion.

ACKNOWLEDGMENTS

The authors thank E.M. Moshkina for assistance and L.A. Solov'ev for valuable discussions.

FUNDING

This study was supported by the Russian Foundation for Basic Research, project NNIO_a no. 21-52-12033).

CONFLICT OF INTEREST

The authors of this work declare that they have no conflicts of interest.

ADDITIONAL INFORMATION

This article is prepared for the memorial issue of the journal dedicated to the 95th birthday of L.A. Prozorova.

REFERENCES

1. A. I. Smirnov, L. E. Svistov, L. A. Prozorova, O. A. Petrenko, and M. Hagiwara, Phys. Usp. **53**, 844 (2010).
2. L. E. Svistov, L. A. Prozorova, N. Büttgen, A. Ya. Shapiro, and L. N. Dem'yanets, JETP Lett. **81**, 102 (2005).
3. A. I. Pankrats, G. A. Petrakovskii, M. A. Popov, K. A. Sablina, L. A. Prozorova, S. S. Sosin, G. Szimczak, R. Szimczak, and M. Baran, JETP Lett. **78**, 569 (2003).
4. J. Schaefer and K. Bluhm, Z. Anorg. Allgem. Chem. **621**, 571 (1995).
5. R. M. Eremina, T. P. Gavrilova, E. M. Moshkina, et al., J. Magn. Magn. Mater. **515**, 167262 (2020).
6. E. Moshkina, C. Ritter, E. Eremin, et al., J. Phys.: Condens. Matter **29**, 245801 (2017).
7. K. Bluhm and H. K. Muller-Buschbaum, Z. Anorg. Allgem. Chem. **582**, 15 (1990).

8. J. Kumar, S. N. Panja, D. J. Mukkattukavil, et al., Phys. Rev. B **95**, 144409 (2017).
9. N. B. Ivanova, M. S. Platunov, Yu. V. Knyazev, N. V. Kazak, L. N. Bezmaternykh, A. D. Vasiliev, S. G. Ovchinnikov, and V. I. Nizhankovskii, Phys. Solid State **54**, 2212 (2012).
10. F. Damay, J. Sottmann, F. Fauth, et al., Appl. Phys. Lett. **118**, 192903 (2021).
11. A. A. Kulbakov, R. Sarkar, O. Janson, et al., Phys. Rev. B **103**, 024447 (2021).
12. M. A. Continentino, J. C. Fernandes, R. B. Guimãraes, et al., Eur. Phys. J.B **9**, 613 (1999).
13. G. A. Petrakovskii, L. N. Bezmaternykh, D. A. Velikanov, A. M. Vorotynov, O. A. Bayukov, and M. Schneider, Phys. Solid State **51**, 2077 (2009).
14. G. M. Sheldrick, Acta Crystallogr., Part A **64**, 112 (2008).
15. *PLATON – A Multipurpose Crystallographic Tool* (Utrecht Univ. Utrecht, The Netherlands, 2008).
16. M. H. Cohen and F. Reif, Solid State Phys. **5**, 321 (1957).
17. I. D. Brown and D. Altermatt, Acta Crystallogr., Part B **41**, 244 (1985).
18. D. A. Velikanov, Inorg. Mater. Appl. Res. **11**, 801 (2020).
19. D. A. Velikanov, Patent RU2481591 (C1), Byull. Izobret. No. 13 (2013).
20. J. C. Fernandes, R. B. Guimarães, M. A. Continentino, et al., Phys. Rev. B **58**, 287 (1998).
21. Y. V. Knyazev, N. V. Kazak, V. S. Zhandun, et al., Dalton Trans. **50**, 9735 (2021).
22. A. P. Douvalis, A. Moukarika, T. Bakas, et al., J. Phys.: Condens. Matter **14**, 3303 (2002).
23. G. A. Bain and J. F. J. Berry, Chem. Educ. **85**, 532 (2008).
24. M. G. Banks, R. K. Kremer, C. Hoch, et al., Phys. Rev. B **80**, 024404 (2009).
25. N. V. Kazak, N. A. Belskaya, E. M. Moshkina, et al., J. Magn. Magn. Mater. **534**, 168056 (2021).

Translated by V. Isaakyan